Bioprinting 21 (2021) e00121

Contents lists available at ScienceDirect

Bioprinting

journal homepage: www.elsevier.com/locate/bprint

3D printed collagen structures at low concentrations supported by jammed microgels

Yifan Zhang [a], S. Tori Ellison [b], Senthilkumar Duraivel [b], Cameron D. Morley [a], Curtis R. Taylor [a], Thomas E. Angelini [a,*]

[a] University of Florida, Department of Mechanical and Aerospace Engineering, Gainesville, FL, 32611, United States
[b] University of Florida, Department of Materials Sciences and Engineering, Gainesville, FL, 32611, United States

ARTICLE INFO

Keywords:
Bioprinting
Extra cellular matrix
3D printing
Biofabrication
Cell infiltration

ABSTRACT

Improving cell infiltration into engineered scaffolds and decelluarized tissue is needed for developing new and effective technologies in regenerative medicine and tissue engineering. Significant challenges associated with populating these structures with cells have persisted for many years. Here we describe a 3D bioprinting method for creating precise structures from natural extracellular matrix at low concentrations that facilitates cell infiltration after printing. We show that when printing collagen-1 solutions into a support medium made from jammed microgels, the printer's basic operating parameters can be used to predict the resulting feature size. Microscopic examination of the printed features show that the collagen solution undergoes gelation and forms a network with the microgels excluded from the printed region. Using this method we 3D print a centimeter-scale model of a developing gut tube and we also show that cells are able to infiltrate printed collagen-1 structures. Our results demonstrate that a diversity of new approaches are possible for creating heterogeneously populated engineered tissue structures.

1. Introduction

The phenotype, health, and function of living cells depend critically on the structure and composition of their 3D microenvironments [1–4]. For example, the promise of tissue engineering strategies that leverage decellularization and re-cellularization technologies hinges upon the idea that pluripotent cells, when placed in the extracellular microenvironment at a specific location within a decellularized tissue, will differentiate into the corresponding phenotype and perform the corresponding function [5]. Similarly, controlled *in vitro* investigations often depend on controlling the structure and composition of extracellular matrix (ECM); morphogenesis in models of developing tissues is extremely sensitive to the details of the extracellular microenvironment [6]. In general, there remain numerous challenges in these areas related to populating 3D extracellular structures with cells, whether the structures are made from decellularized tissue, purified ECM gels like collagen-1, or synthetic polymers. To facilitate research in stem cell differentiation, tissue fabrication, and developmental models, researchers need new methods for easily structuring natural and synthetic ECM in 3D that can be infiltrated by cells. In this brief communication, we focus on structuring purified collagen-1, yet the method we describe below can be extended to many other ECM materials, whether natural or synthetic.

3D bioprinting represents one potential class of tools capable of structuring ECM with few restrictions. For many years in the 3D bioprinting field, a great deal of focus has been placed on methods for printing layer-by-layer in air, similar to thermoplastic extrusion employed in the most commonly found 3D printers [7–10]. The instabilities associated with extruding fluid elements into air, even when supported by rigid substrates, have driven the innovated development of self-supporting "bio-inks" [11]. For example, surface and body forces that cause structures to spread or sag can be overcome by increasing ECM concentration, by mixing with additives like alginate, nanoclays, or nanocrystals, or by printings single layers onto surfaces with low adhesion [12–18]. Some approaches side-step the need for self-supporting bio-inks by printing sacrificial molds then filling with ECM [19]. While these materials have exhibited biocompatibility and printability, the sensitivity of cells to the physical and chemical details of their microenvironments creates additional concerns about using these innovative materials. By contrast, new methods for 3D printing natural ECM with no modifications will enable researchers to use established understanding of

* Corresponding author.
E-mail address: t.e.angelini@ufl.edu (T.E. Angelini).

https://doi.org/10.1016/j.bprint.2020.e00121
Received 9 August 2020; Received in revised form 5 December 2020; Accepted 8 December 2020

cell-matrix interactions in tissue fabrication strategies, whether for fundamental research or for technological applications. While some demonstrations of natural ECM printing exist, they often do not explore the manufacturing variable-space needed to test the limitations of the methods [20], or they involve cell-laden inks [21]. To facilitate and encourage the use of 3D bioprinting by a broad base of users who lack access to specialized bioinks or have concerns about their biological relevance, work must be done to establish that natural ECM can be 3D printed with predictable feature-sizes while working at concentrations typically used in 3D cell culture applications.

In this brief communication, we describe a method for 3D printing large-scale ECM structures made from collagen-1 at the relatively low concentrations often used in 3D culture. We leverage a recently developed 3D printing support medium made from jammed granular-scale microgels [21–26], which was previously used to fabricate structures made from synthetic hydrogels, living cells, and silicone elastomers. Granular-scale microgels are hydrogel particles having diameters greater than 1 μm and typically less than 20 μm; they are jammed when tightly packed together, forming a solid-like phase [23,27,28]. While ECM was previously included in some cell prints, the efficacy of ECM printing in terms of fabrication control, quality, and cell infiltration after printing has yet to be demonstrated. Here, we find that printed collagen features have circular cross-sections of radius, R, which can be controlled by the volumetric material deposition rate, Q, and translation speed, V. By varying both Q and V independently, we find the feature size is predicted by the simple continuity relationship, $\pi R^2 = Q/V$ under a range of operating conditions. Confocal reflectance microscopy measurements confirm that the collagen-1 solutions form fibrous networks resembling those produced with traditional gelation protocols. Additionally, we find that microgels are expelled from the locations where collagen is deposited with very little apparent intermixing between the two materials. We design and print models of the developing gut to show the ability to support free-form structures, and we show that cells can infiltrate these structures from the surrounding microgel support medium.

2. Results and discussion

To explore the effectiveness of 3D printing structures made from low-concentration ECM into jammed microgel support media, we inject solutions of refrigerated, acidic, bovine collagen-1 into the microgel medium using a syringe needle moving in 3D paths (see Methods and Materials for details). We hypothesized that the microgel support medium will enable 3D printing of well-defined and predictable features that are not possible when printing in open air onto solid substrates, where interfacial and body forces drive fluid spreading, interfacial instabilities, and sagging (Fig. 1). Briefly, the microgel medium is formulated to have a yield stress of 15 Pa by mixing Carbomer 980 powder into ultrapure water and neutralizing the mixture with sodium hydroxide (NaOH), setting the final polymer concentration to 0.15%. A yield stress of 15 Pa is low enough to prevent crevices from forming in the wake of the translating syringe needle, which are observed when using support materials with higher yield stresses [23]. We previously published rheological characterizations of Carbomer 980 and many other microgel formulations, so we do not include the repeated data in this brief communication [24,27]. With our formulation, the hydrostatic pressure at just 9 mm below the surface is high enough to yield the jammed microgels and facilitate flow, continuously filling the space behind the translating needle while surrounding and supporting the printed features. The collagen solution is prepared by diluting commercially available Type I bovine collagen at 5.8 mg/mL down to 1.9 mg/mL using 1× Dulbecco's Modification of Eagle's Medium solution. To facilitate measuring feature diameters, the collagen solution is mixed with toluidine blue dye at a final concentration of 40 ppm. The collagen solution is loaded into a 1 mL syringe fitted with a 30-gauge, 1-inch long needle and

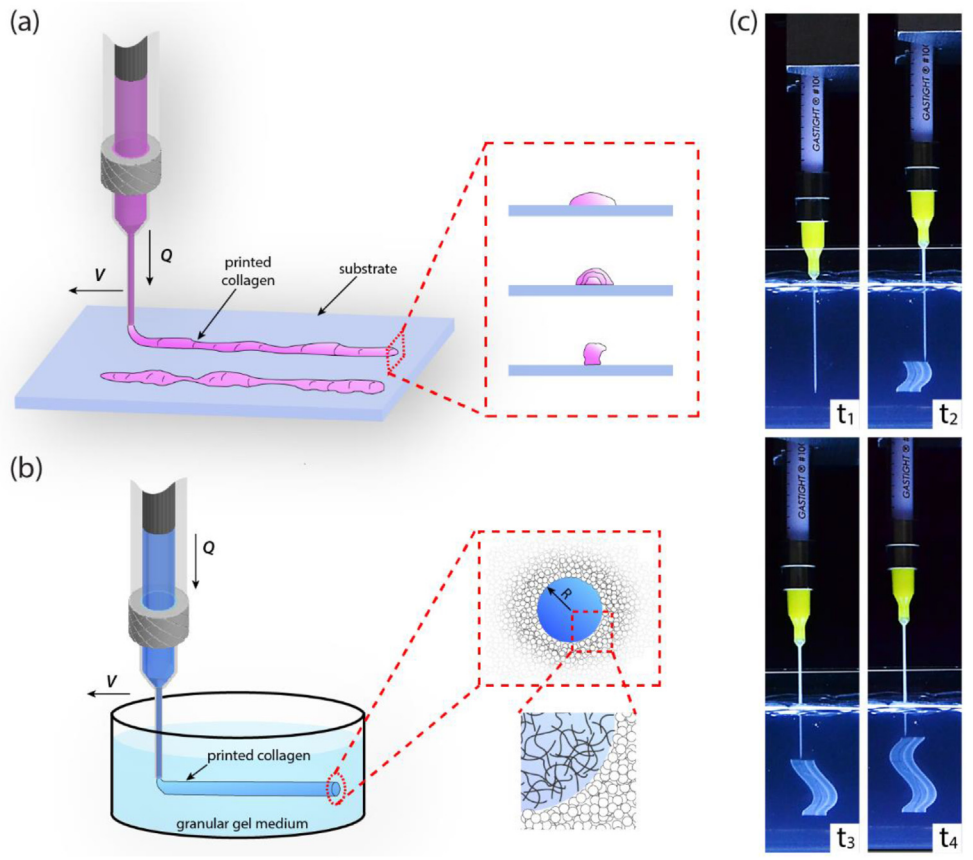

Fig. 1. Low-concentration ECM printed in air and microgel medium. (a) A syringe needle printing a simple linear feature at flow rate, Q, and translation speed, V, onto a solid substrate in open air will produce unstable features that spread and slump. (b) The same feature when printed into granular microgel medium under the same conditions, is stable and controllable; as the needle moves, the material is deposited into the microgel medium which continuously surrounds and supports the printed feature. The printed ECM material forms a gelled network, structured within the microgel medium. (c) Macro-images of the printing process, described in more detail later in the manuscript.

mounted onto our 3D printing instrument (Fig. 1c).

The 3D printing approach described here employs an aqueous collagen-1 ink and an aqueous microgel support medium, essentially eliminating interfacial tension between the two materials. Given the lack of a two-phase solvent interface between these materials, it is natural to expect intermixing between the collagen and microgel materials. To qualitatively test the extent of intermixing between the support medium and the collangen-1 ink, we perform experiments in which we mix the microgels with 4.8 μm diameter fluorospheres before printing and look for an effective interface between the printed feature and the surrounding microgel medium, indicated by the distribution of the fluorescent fiducial markers. Thin XY slices from confocal fluorescence microscopy stacks show relatively sharp interfaces between the surrounding medium and the printed features, where very little gradient in fluorescent particle density is observed and only the occasional stray particle is found within the printed feature region (Fig. 2a). Cross-sectional projections in the X-Z plane show remarkably circular cross-sections (Fig. 2b). To test whether the collagen-1 solutions form gelled networks after printing into the 37 °C medium at neutral pH, we print features near the base of glass-bottomed petri-dishes and perform confocal reflectance microscopy measurements using a 60× oil-immersion objective. These measurements confirm that polymerized gels form within 40 min after printing (Fig. 2c). A broader range of collagen concentrations (0.25–2 mg/mL) were previously shown to polymerize under similar printing conditions, expanding the potential range of constructs that could be made beyond that described here [21]. To test our ability to control the diameter of printed features, we vary the translation speed, V, and material deposition rate, Q, and fabricate linear features within the microgel medium. We perform bright-field microscopy using Koeller illumination with a small condenser aperture to enhance contrast between the printed feature and the surrounding microgel medium; the presence of toluidine blue dye in the collagen ink further enhances contrast. With this method we are able to identify printed features and show that larger features are produced by decreasing V or increasing Q (Fig. 2 d-f).

To quantify the relationship between feature size and printing parameters, we perform a series of tests like those described above, in which we vary the needle translation speed, V, and the material deposition rate, Q. We vary V between 0.1 and 1 mm/s; we vary Q between 50 and 500 μL/h. The diameters of printed features are measured from bright field images collected as described above. Given the circular cross-sections found from confocal microscopy measurements, we treat the diameters measured in cross-section as representative of the average diameter, from which we compute the cross-sectional area of features as $A = \pi R^2$, where R is the feature radius. Overall, we find that A is nearly proportional to Q and nearly inversely proportional to V within s sub-set of printing conditions (Fig. 3 a,b). We note that fewer data points are shown for experiments performed at the highest and lowest speeds and flow-rates; at these extreme conditions, the printed shapes are sometimes irregular or intermittent, so we are unable to measure R. For the printing conditions where R is measurable, we expect these general trends to be predicted by simple incompressible fluid continuity, $\pi R^2 = Q/V$. To test the extent to which this continuity relationship holds, we pool all the data and plot πR^2 versus Q/V (Fig. 3c). We find that features produced using most printing conditions explored here lay close to this prediction; features generated at the highest speed of 1 mm/s fall far from the prediction. These results demonstrate the range of instrumental fabrication parameters that enable predicable 3D printing of collagen features.

In recent work, we demonstrated our ability to use this general approach for 3D printing simple linear and sheet-shaped features at the small-scale, made from mixtures of living cells and collagen-1 [21]. By contrast, this method has never been shown to be capable of producing complex shapes made from cell-free collagen-1 networks at the large-scale. To demonstrate this capability, we produce basic geometric models of the developing gut tube, which consists of a hollow cylinder connected to a thin sheet that lays along the cylinder's axis [29,30]. During development, the gut tube undergoes a buckling transition driven by the combination of cell-generated expansion of the tube resisted by the elasticity of the attached sheet. We generate models of the straight gut tube and the buckling gut tube in a helical conformation using 3D CAD models software Solidworks 2016. The cross-sectional sketch is made by overlapping a rectangular (4 mm × 0.3 mm) on a circle with 1.5 mm radius. The sketch is then extruded along a straight path or swept

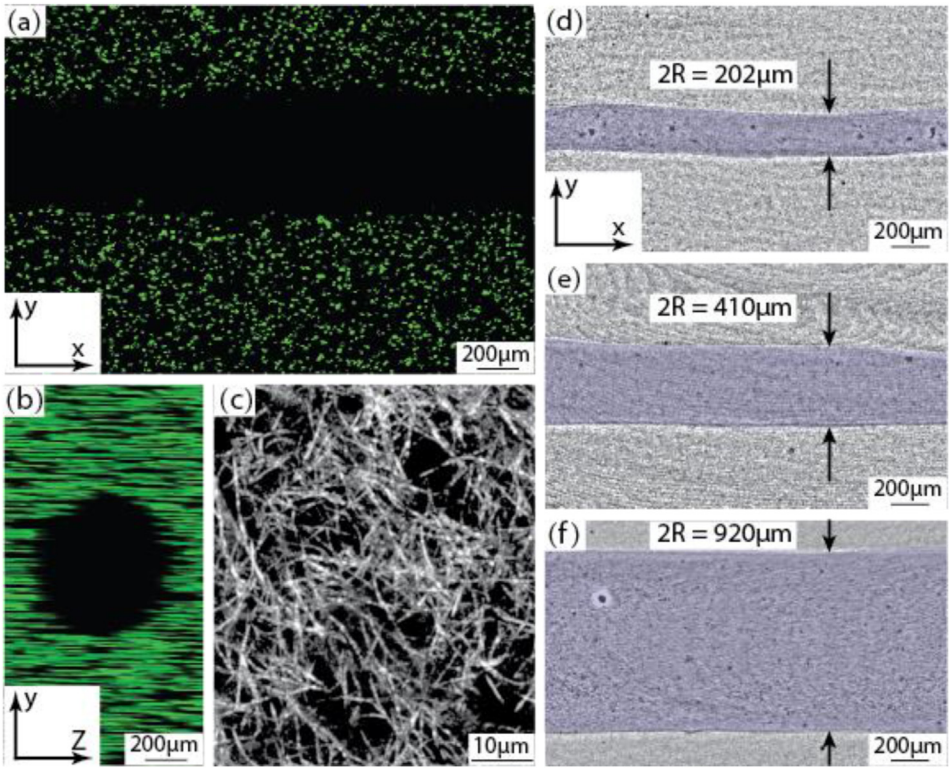

Fig. 2. Printed feature in microgel medium. (a,b) Here we show a bottom view (XY slice) and a cross-sectional view (YZ slice) of collagen ink printed into microgels mixed with fluorospheres. The dark regions contain printed collagen and the green speckled regions contain microgels mixed with fluorospheres. (c) Confocal reflectance microscopy demonstrates the formation of gelled networks of printed collagen within the microgel medium. (d–f) The bottom view of polymerized collagen (false-colored blue regions) in microgels show varying feature diameter with different printing conditions. The collagen features are printed under the following conditions: Q = 50 μL/h and V = 0.5 mm/s (d); Q = 125 μL/h and V = 0.25 mm/s (e); and Q = 500 μL/h and V = 0.25 mm/s (f). (For interpretation of the references to color in this figure legend, the reader is referred to the Web version of this article.)

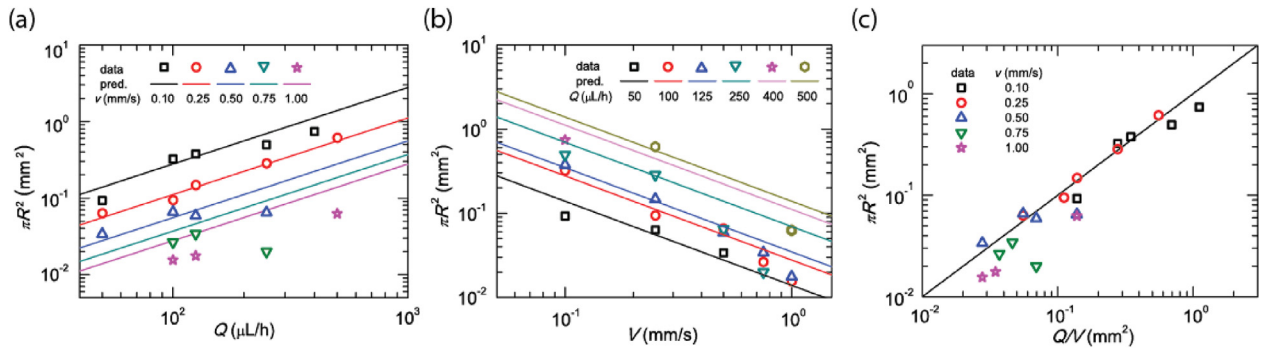

Fig. 3. Quantitative results of printed feature diameters. (a) The cross-sectional areas of collagen features increase with increasing Q at different V. (b) The cross-sectional areas of features decrease with increasing V at different Q. (c) The cross-sectional areas of features are well predicted by the continuity relationship, $\pi R^2 = Q/V$, for most printing conditions and deviate strongly from the prediction for large V.

along a curved path to form the two gut-tube models. The model is exported as an STL file and imported into a commercial slicing software, Cura 2.7.0, to generate G code, which can be executed by 3D printer. The gut tube models are printed following the procedures described above and using a flow rate $Q = 100$ μL/h and a translation speed $V = 2$ mm/s. We perform macro-photography to image the 1 cm long structures while still embedded in the microgel medium. To provide a large population of light-scattering centers that create contrast to facilitate photography, we pre-mix the collagen-1 solution with microspheres 4.8 μm in diameter at a concentration of approximately 1.25% by volume. Direct comparison between the photographs and renderings of the CAD models show good reproduction of the designed structures, viewed from several different angles (Fig. 4). In Fig. 4, we only show macro-scale images because the size of the printed objects, the thickness of the quartz glass vessel they are printed in, and the distance between the walls of the vessel and the printed objects, together, make microscopic imaging impossible. Thus, the micro-scale experiments described above, in which we print selected features very close to the bottom of a glass-bottomed Petri dish and image at high magnification, serve to verify the micro-scale quality of these macro-scale structures. Given the quality of these structures, we foresee that in the future it will be possible to 3D print cell-free scaffolds from ECM that can be later infiltrated by cells.

To test whether cells will spontaneously infiltrate 3D printed structures, we seed the microgel medium with fluorescently dyed NIH 3T3 fibroblasts before printing the collagen-1 structure. We print simple linear features, made of 2 mg/mL collagen-1, oriented horizontally near the bottom of glass-bottom petri dishes to enable imaging in confocal fluorescence microscopy. In these experiments, the microgels are synthesized from polyacrylamide and methacrylic acid, and swollen to 2.2% polymer (w/w) in DMEM cell growth medium. The suitability of these microgels, the Carbopol 980 microgels, and several other types of microgel, for cell culture applications and 3D printing have been shown previously [21,28]. Immediately after printing, we find that the cells are pushed out of the printing area, as expected from the experiments described above where the same phenomenon occurs with fluorosphere-seeded microgel media (Fig. 5a). After 24 h, we find that the printed regions are infiltrated with cells (Fig. 5b). We find that the cells within the printed region extend dramatically compared to the cells residing in the microgels outside the printed region. The extended morphology of these fibroblasts is consistent with that of cells embedded in a collagen-1 matrix, as we observed previously when printing mixtures of fibroblasts and collagen-1. By contrast, cells outside the printed region remain round, most likely associated with the absence of adhesive ligands found in ECM that are necessary for integrin-mediated anchoring.

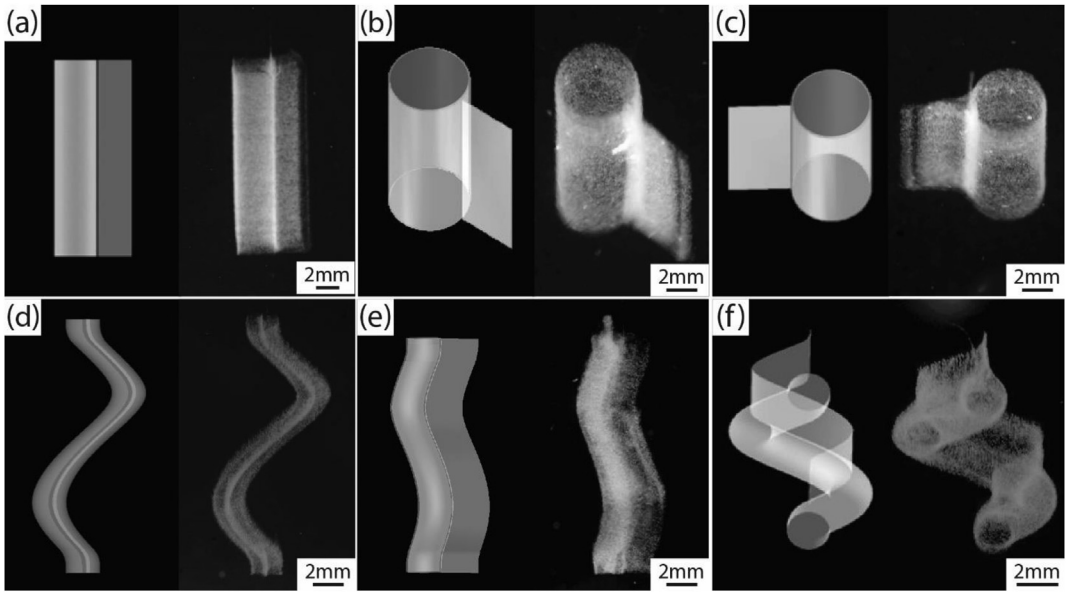

Fig. 4. 3D printed models of a straight and helical gut tube during development. (a–c) The developing gut tube consists of a hollow cylinder attached to a sheet, connected along the cylinder's axis. We first created a straight model of the developing gut tube. Each panel shows a different perspective of the CAD model (left) and the 3D printed structure (right). (d–f) As the gut-tube develops *in vivo*, it buckles, which we model here as a helix (CAD models on left; 3D printed models on right). The side view of a helix is a sinusoid, which is apparent in (d) and (e). The skewed perspective (f) shows the helical structure.

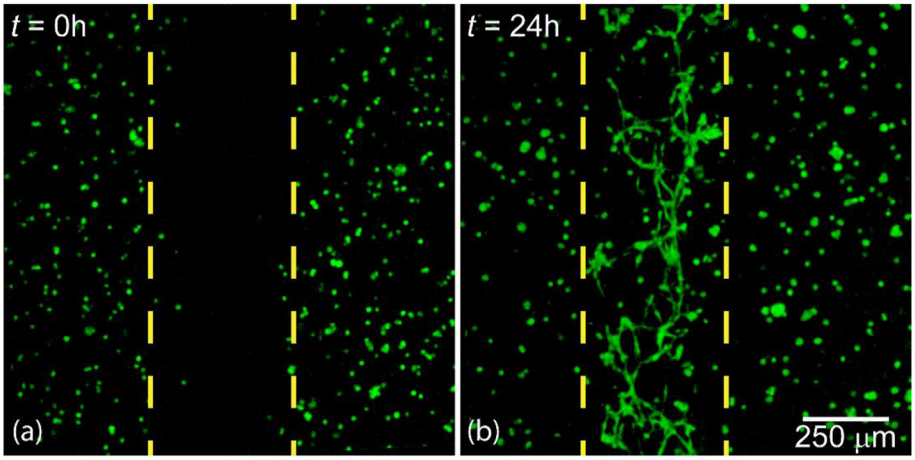

Fig. 5. Cell infiltration into 3D printed collagen networks. (a) Prior to printing collagen-1 features, the microgel medium is seeded with NIH 3T3 fibroblasts. Immediately after printing, we find that cells are pushed out of the printing region as expected from previous experiments with fluorosphere-loaded microgels. (b) After 24 h of incubation, cells infiltrate the printed region and take on an extended morphology, as expected from fibroblasts embedded in a collagen-1 network. Cells outside the printed feature remain round, as they are unable to perform integrin-mediated adhesion because of the absence of integrin-binding ligands in the microgel medium.

3. Conclusion and outlook

The bioprinting method described here represents the potential to create precise structures from natural ECM at low concentrations, facilitating the infiltration of cells into a matrix without the need for specialized bioinks, synthetic matrices, or chemically modified biopolymers. Printing collagen-1 directly into microgels results in structures with well-defined features; within a range of operating parameter space, the radii of printed collagen features is well predicted by a simple balance of volumetric flow-rate, Q, and needle velocity, V, given by $\pi R2 = Q/V$. We observe that the microgel support medium surrounds and supports the collagen features in a nearly perfect cylindrical shape and does not appear to intermix with the collagen during printing or gelation. In principle, the same strategy could be taken to print other types of ECM such as hyaluronic acid, laminin, fibronectin, or ECM mixtures like Matrigel.

While we have emphasized the value of our method when printing low concentration ECM solutions, some applications require high ECM concentrations, like when printing mimics of cardiac tissue [31]. In such applications or any others employing concentrated biopolymer solutions, one of the most significant challenges is the strongly shear-thinning properties of these ink materials. Strongly shear-thinning inks create challenges when using pressure driven flows, since the viscosities of these concentrated inks can change dramatically with flow rate. This varying viscosity creates the need for closed-loop control over applied pressure in response to changes in flow-rate. The method described here avoids these challenges because flow rates are controlled by the displacement of a rigid syringe plunger within a rigid syringe barrel; the flow rates do not vary as a function of the changing ink viscosity that shear-thinning materials exhibit. This displacement-controlled approach has been shown to work with strongly shear-thinning inks like high concentration solutions of aqueous polymer and silicone elastomer precursors [23,32].

We foresee using the method described here to facilitate precise cell infiltration approaches to be developed. Dispersed cells could first be printed without ECM – whether monocultures or multiple different cell types placed in different locations – and subsequently ECM could be printed into detailed structures right within the dispersed cell populations. Our previous work shows the efficacy of printing cells without ECM [22,23]. The results shown here indicate that during the ECM printing step, the cells will be pushed to the periphery of the deposited ECM structures, with some population close enough to touch the ECM and guide their infiltration. As an example, the gut-tube model here could be fabricated in this way; a helical tube of epithelial cells could be printed, followed by the collagen structure we printed in this work. In such a case, it may be possible to drive the cells to infiltrate only into the tube portion but not into the attached sheet because of their chosen proximity to the different parts of the structure. Variations of this approach could be used by researchers focused on soft scaffold printing or mechanically mediated interactions between cells and ECM, or more broadly in studies of 3D cell growth and migration. For example, this approach could be used to drive stem cell differentiation in 3D with spatial control; printing collagen at different concentrations into homogeneous distributions of stem cells could be used to create heterogeneously functioning tissue as was seen when culturing mesenchymal stem cells on collagen substrates having different elastic moduli [33]. While the method described in this brief communication was limited to collagen-1 networks and fibroblasts, our results show that diverse studies of different ECMs and cell types are feasible.

4. Methods and materials

4.1. Carbomer microgel preparation

To prepare microgel for 3D printing, 0.15 wt% Carbomer 980 power (Lubrizol Co.) is dispersed into ultrapure water (18.2 Mohm-cm). An appropriate amount of 10× NaOH is added to the medium to adjust pH to 7. The final microgel medium is mixed by a high-speed centrifugal mixer at 3500 rpm for 5 min. For fluorescent bead exclusion tests performed with confocal microscopy, we add 3 wt% green fluorescent microspheres having 4 μm diameters (Thermo Scientific).

4.2. Polyacrylamide - methacrylic acid microgel synthesis

Lightly crosslinked polyacrylamide microgels with 17 mol% methacrylic acid as an ionizable comonomer are prepared according to a previous report[16]. A solution of 8% (w/w) acrylamide, 2% (w/w) methacrylic acid, 1% (w/w) poly (ethylene glycol) diacrylate (MW = 700 g mol^{-1}), and 0.1% (w/w) azobisisobutyronitrile in ethanol (490 mL) is prepared. The solution is sparged with nitrogen for 30 min, then placed into a preheated oil bath set at 60 °C. After approximately 30 min, the solution becomes hazy and a white precipitate begins to form. The reaction mixture is heated for an additional 4 h. At this time, the precipitate is collected by vacuum filtration and rinsed with ethanol on the filter. The microparticles are triturated with 500 mL of ethanol overnight. The solids are again collected by vacuum filtration and dried on the filter for 10 min. The particles are dried completely in a vacuum oven set at 50 °C to yield a loose white powder. The purified microgel powder is dispersed in cell growth media at various concentrations and mixed at 3500 rpm in a centrifugal speed mixer[1,2] in 5-min intervals until no aggregates are apparent. The microgel is then neutralized to a pH of 7.4 with NaOH and 25 mM HEPES buffer (part no. BP299-100) and is left to swell overnight, yielding microgel 3D printing and growth media at polymer concentrations of 2.2% (w/w).

4.3. Printed collagen preparation

To prepare the collagen solution, 6.1 mg/mL Type I bovine collagen solution (Advanced BioMatrix) is diluted to 2 mg/mL by adding appropriate amount of 1× Dulbecco's Modification of Eagle's Medium (DMEM, Mediatech, Inc.). HEPES is added to the solution to adjust the pH to 7.4. To visualize the printed collagen with brightfield microscopy we add toluidine blue (TB) dye solution to the collagen solution at a final concentration of 0.4% by volume. Collagen is printed into the microgel medium and gelled at 37 °C and 5% CO_2 for 40 min. When printing the gut structures, TB dye solution is substituted by 1.25 vol% polystyrene microspheres (Thermo Scientific).

4.4. 3D printing collagen into the microgel medium

The 3D printing instrument is a custom-built 3D printer with 1 μm repeatability in the XYZ directions and a custom-built syringe pump. The pump and the stages are coupled together and programmed by G code to print collagen solutions at chosen flow rates and velocities. The injection needle tips used when printing collagen lines and gut structures are 27G and 30G blunt-tipped stainless steel needles, respectively. The gut structures are modeled by SOLIDWORKS 2016 and coded by Cura 2.7.0.

4.5. Cell culture and 3D bioprinting

NIH-3T3 fibroblast cells are cultured in Dulbecco's Modified Eagle Medium (DMEM) with 4.5 g/L glucose, L-glutamine, and sodium pyruvate supplemented with 10% FBS and 1% penicillin streptomycin. When the cells have reached 70% confluence, they are dyed with cell tracker green (CMFDA) (Thermo-Fisher, part no. C2925), washed with PBS, and incubated in 3 mL of 5% Trypsin - EDTA solution for 5 min. The cells are harvested from the plate and placed into a 15 mL centrifuge tube, where they are centrifuged at 2000 rpm for 3 min. The supernatant is removed from the tube and 200 μL of cell growth media is added. The cell pellet is dispersed with gentle pipette mixing and the solution is pipetted into 1.5 mL of the microgel culture medium prepared with the corresponding cell growth media at 2.2% (w/w). The mixture is placed in a glass bottom 35-mm Petri dish and incubated at 37 °C and 5% CO_2 for 1–2 h.

Bovine collagen-1 (Advanced BioMatrix, part no. 5010-50 ML) is diluted to 2 mg/mL, loaded into a 100 μL Hamilton gas-tight syringe, and a sterile, blunt-tip 30 gauge luer-lock needle (SAI, part no. B30-50) is affixed to the syringe. The syringe is mounted onto our printer and the collagen is printed into the microgel-cell mixture in straight lines at a velocity of 0.1 mm/s and flow rate of 100 μL/h. The structures are imaged on a Nikon Eclipse Ti-E microscope with a C2 confocal scanning system at time points 0 and 24 h. The images are processed using FIJI.

4.6. Photography and microscopy

Photographs are taken using a Nikon D3X or a Nikon D800 camera under ambient lighting. Micrographs are taken by a Nikon Eclipse Ti-E microscope with a C2 confocal scanning system. All images are processed using Fiji.

CRediT authorship contribution statement

Yifan Zhang: Methodology, Investigation, Data curation, Software, Visualization, Writing. **S. Tori Ellison:** Methodology, Investigation, Data curation, Software, Visualization, Writing. **Senthilkumar Duraivel:** Investigation, Data curation, Software, Visualization. **Cameron D. Morley:** Methodology, Investigation, Data curation, Software, Visualization. **Curtis R. Taylor:** Supervision, Project administration. **Thomas E. Angelini:** Conceptualization, Writing, Supervision, Project administration.

Declaration of competing interest

The authors declare that they have no known competing financial interests or personal relationships that could have appeared to influence the work reported in this paper.

Acknowledgement

This material is based on work supported by the National Science Foundation under grant no. DMR-1352043.

References

[1] B.M. Baker, C.S. Chen, Deconstructing the third dimension–how 3D culture microenvironments alter cellular cues, J. Cell Sci. 125 (13) (2012) 3015–3024.
[2] E. Cukierman, R. Pankov, D.R. Stevens, K.M. Yamada, Taking cell-matrix adhesions to the third dimension, Science 294 (5547) (2001) 1708–1712.
[3] S.I. Fraley, Y. Feng, R. Krishnamurthy, D.-H. Kim, A. Celedon, G.D. Longmore, D. Wirtz, A distinctive role for focal adhesion proteins in three-dimensional cell motility, Nat. Cell Biol. 12 (6) (2010) 598–604.
[4] D.W. Hutmacher, Biomaterials offer cancer research the third dimension, Nat. Mater. 9 (2) (2010) 90–93.
[5] S.F. Badylak, D. Taylor, K. Uygun, Whole-organ tissue engineering: decellularization and recellularization of three-dimensional matrix scaffolds, Annu. Rev. Biomed. Eng. 13 (2011) 27–53.
[6] C.M. Nelson, M. Bissell, Of extracellular matrix, scaffolds, and signaling: tissue architecture regulates development, homeostasis, and cancer, Annu. Rev. Cell Dev. Biol. 22 (2006) 287–309.
[7] S. Yoon, J.A. Park, H.R. Lee, W.H. Yoon, D.S. Hwang, S. Jung, Inkjet-spray hybrid printing for 3D freeform fabrication of multilayered hydrogel structures, Adv Healthc Mater 7 (14) (2018).
[8] N.E. Fedorovich, J. Alblas, J.R. de Wijn, W.E. Hennink, A.J. Verbout, W.J.A. Dhert, Hydrogels as extracellular matrices for skeletal tissue engineering: state of the art and novel application in organ printing, Tissue Eng. 13 (8) (2007) 1905–1925.
[9] B.S. Kim, J.S. Lee, G. Gao, D.W. Cho, Direct 3D cell-printing of human skin with functional transwell system, Biofabrication 9 (2) (2017).
[10] J. An, J.E.M. Teoh, R. Suntornnond, C.K. Chua, Design and 3D printing of scaffolds and tissues, Eng. Plast. 1 (2) (2015) 261–268.
[11] F. You, B.F. Eames, X. Chen, Application of extrusion-based hydrogel bioprinting for cartilage tissue engineering, Int. J. Mol. Sci. 18 (7) (2017).
[12] Y. Tan, D.J. Richards, T.C. Trusk, R.P. Visconti, M.J. Yost, M.S. Kindy, C.J. Drake, W.S. Argraves, R.R. Markwald, Y. Mei, 3D printing facilitated scaffold-free tissue unit fabrication, Biofabrication 6 (2) (2014).
[13] Y.F. Jin, D.Y. Zhao, Y. Huang, Study of extrudability and standoff distance effect during nanoclay-enabled direct printing, Bio-Des Manuf 1 (2) (2018) 123–134.
[14] Y.F. Jin, Y.Y. Shen, J. Yin, J. Qian, Y. Huang, Nanoclay-based self-supporting responsive nanocomposite hydrogels for printing applications, ACS Appl. Mater. Interfaces 10 (12) (2018) 10461–10470.
[15] Y.N. Jiang, J.P. Zhou, Z. Yang, D.F. Liu, X.D. Xv, G.Q. Zhao, H.C. Shi, Q. Zhang, Dialdehyde cellulose nanocrystal/gelatin hydrogel optimized for 3D printing applications, J. Mater. Sci. 53 (16) (2018) 11883–11900.
[16] K. Jakab, C. Norotte, B. Damon, F. Marga, A. Neagu, C.L. Besch-Williford, A. Kachurin, K.H. Church, H. Park, V. Mironov, R. Markwald, G. Vunjak-Novakovic, G. Forgacs, Tissue engineering by self-assembly of cells printed into topologically defined structures, Tissue Eng. 14 (3) (2008) 413–421.
[17] V. Mironov, R.P. Visconti, V. Kasyanov, G. Forgacs, C.J. Drake, R.R. Markwald, Organ printing: tissue spheroids as building blocks, Biomaterials 30 (12) (2009) 2164–2174.
[18] K. Jakab, A. Neagu, V. Mironov, R.R. Markwald, G. Forgacs, Engineering biological structures of prescribed shape using self-assembling multicellular systems, P Natl Acad Sci USA 101 (9) (2004) 2864–2869.
[19] C.Z. Liu, Z.D. Xia, Z.W. Han, P.A. Hulley, J.T. Triffitt, J.T. Czernuszka, Novel 3D collagen scaffolds fabricated by indirect printing technique for tissue engineering, J. Biomed. Mater. Res. B 85b (2) (2008) 519–528.
[20] T.J. Hinton, Q. Jallerat, R.N. Palchesko, J.H. Park, M.S. Grodzicki, H.-J. Shue, M.H. Ramadan, A.R. Hudson, A.W. Feinberg, Three-dimensional printing of complex biological structures by freeform reversible embedding of suspended hydrogels, Science advances 1 (9) (2015), e1500758.
[21] C.D. Morley, S.T. Ellison, T. Bhattacharjee, C.S. O'Bryan, Y. Zhang, K.F. Smith, C.P. Kabb, M. Sebastian, G.L. Moore, K.D. Schulze, Quantitative characterization of 3D bioprinted structural elements under cell generated forces, Nat. Commun. 10 (1) (2019) 1–9.
[22] T. Bhattacharjee, C.J. Gil, S.L. Marshall, J.M. Uruena, C.S. O'Bryan, M. Carstens, B. Keselowsky, G.D. Palmer, S. Ghivizzani, C.P. Gibbs, Engineering, Liquid-like solids support cells in 3D, ACS Biomaterials Science 2 (10) (2016) 1787–1795.
[23] T. Bhattacharjee, S.M. Zehnder, K.G. Rowe, S. Jain, R.M. Nixon, W.G. Sawyer, T.E. Angelini, Writing in the granular gel medium, Science advances 1 (8) (2015), e1500655.
[24] C.S. O'Bryan, T. Bhattacharjee, S.L. Marshall, W.G. Sawyer, T.E. Angelini, Commercially available microgels for 3D bioprinting, Bioprinting 11 (2018), e00037.

[25] W. Cheng, J. Zhang, J. Liu, Z. Yu, Granular hydrogels for 3D bioprinting applications, View 1 (3) (2020) 20200060.
[26] A. McCormack, C.B. Highley, N.R. Leslie, F.P.W. Melchels, 3D printing in suspension baths: keeping the promises of bioprinting afloat, Trends Biotechnol. 38 (6) (2020) 584–593.
[27] T. Bhattacharjee, C.P. Kabb, C.S. O'Bryan, J.M. Urueña, B.S. Sumerlin, W.G. Sawyer, T.E. Angelini, Polyelectrolyte scaling laws for microgel yielding near jamming, Soft Matter 14 (9) (2018) 1559–1570.
[28] C.S. O'Bryan, C.P. Kabb, B.S. Sumerlin, T.E. Angelini, Jammed polyelectrolyte microgels for 3D cell culture applications: rheological behavior with added salts, ACS Applied Bio Materials 2 (4) (2019) 1509–1517.
[29] N.L. Nerurkar, L. Mahadevan, C.J. Tabin, BMP signaling controls buckling forces to modulate looping morphogenesis of the gut, Proc. Natl. Acad. Sci. Unit. States Am. 114 (9) (2017) 2277–2282.
[30] T. Savin, N.A. Kurpios, A.E. Shyer, P. Florescu, H. Liang, L. Mahadevan, C.J. Tabin, On the growth and form of the gut, Nature 476 (7358) (2011) 57–62.
[31] A. Lee, A. Hudson, D. Shiwarski, J. Tashman, T. Hinton, S. Yerneni, J. Bliley, P. Campbell, A. Feinberg, 3D bioprinting of collagen to rebuild components of the human heart, Science 365 (6452) (2019) 482–487.
[32] C.S. O'Bryan, T. Bhattacharjee, S. Hart, C.P. Kabb, K.D. Schulze, I. Chilakala, B.S. Sumerlin, W.G. Sawyer, T.E. Angelini, Self-assembled micro-organogels for 3D printing silicone structures, Science advances 3 (5) (2017), e1602800.
[33] A.J. Engler, S. Sen, H.L. Sweeney, D.E. Discher, Matrix elasticity directs stem cell lineage specification, Cell 126 (4) (2006) 677–689.